Journal of Alloys and Compounds 503 (2010) 82–85

Contents lists available at ScienceDirect

Journal of Alloys and Compounds

journal homepage: www.elsevier.com/locate/jallcom

Pure red upconversion emission from $Yb_3Al_5O_{12}$ phase doped with high Er^{3+} concentration

Xu Changfu[a,b], Yang Qibin[a,b,*], Ren Guozhong[b], Liu Yunxin[a]

[a] Institute of Modern Physics, Faculty of Material & Photoelectronic Physics, Xiangtan University, Xiangtan 411105, China
[b] Key Laboratory of Low Dimensional Materials & Application Technology of Ministry of Education, Xiangtan University, Xiangtan 411105,China

ARTICLE INFO

Article history:
Received 4 November 2009
Received in revised form
30 December 2009
Accepted 30 December 2009
Available online 6 January 2010

Keywords:
$Yb_3Al_5O_{12}$ (YbAG)
Pure red upconversion emission

ABSTRACT

Pure red upconversion luminescence was observed from Er^{3+} doped $Yb_3Al_5O_{12}$ powder synthesized by sol–gel method. X-ray diffraction (XRD) and transmission electron microscopy (TEM) patterns revealed two phases $Yb_3Al_5O_{12}$ and Yb_2O_3 coexisting as crystals. High resolution transmission electron microscopy (HRTEM) and energy dispersive spectroscopy (EDS) analysis showed that the luminescence was from Er^{3+} in $Yb_3Al_5O_{12}$. High pure red emission was obtained in all three samples with the emission intensity ratios of red to green (R/G) being 78, 110 and 136 respectively. It was found that Yb^{3+} was a composition of the host $Yb_3Al_5O_{12}$ rather than a doped ion and still played a sensitizing role and the R/G was in a positive variation with the ratio of Yb^{3+}/Er^{3+}. The possible mechanism can be ascribed to the resonant energy transfer $^4F_{7/2}(Er^{3+}) + {}^4I_{11/2}(Er^{3+}) \rightarrow 2{}^2F_{9/2}(Er^{3+})$ caused by the high content of Yb^{3+}.

1. Introduction

The research of rare earth ion doped energy upconversion materials has triggered active interest for its potential applications in the optical devices such as color display, planar waveguides, communication fibers and immunoassay [1–6]. The fact that the rare earth ions have a plenty of energy levels provoking these ions emitting a wide range spectra covering near infrared (NIR) to ultraviolet (UV), however, this excellent phenomenon itself means a negative point which makes it difficult to obtain single color emission such as pure red upconversion emission which has potential applications in color display and visual search [7]. Dong, Liu, et al. [8–12] reported high emission intensity ratio of the red to the green (R/G) in Er^{3+}/Yb^{3+} co-doped upconversion materials with the excitation of 980 nm LD, but the purity was not high enough. Liu et al. [9,13] reported that the high concentration of Yb^{3+} ion would bring high value of R/G. According to the Bai et al. [14], it is possible to obtain single color upconversion emission when the concentration of Yb^{3+} and Er^{3+} ions is optimized. High purity of green emission was also found in rare earth doped in Y_2O_3 [15,16], Gd_2O_3 [17] and $SrTiO_3$ [18] powders by optimization of dopant ions. Shen et al. [19] reported high ratio of green to red in TeO_2 glass under different wavelength (973 and 800 nm) LD excitation.

Much attention were paid to Er^{3+}/Yb^{3+} co-doped materials where Er^{3+} play a role as a luminescence center, while Yb^{3+} as sensitizing agent to enhance efficiency of emission of Er^{3+} because the relative low absorption cross-section of Er^{3+} makes the ground state absorption weakly, but Yb^{3+} has a much greater absorption cross-section. Energy transfer from Yb^{3+} ions to Er^{3+} ions enhances the efficiency of the upconversion emission drastically [20,21]. Although fluoride [22] and tellurite [23] with low phonon energy attracted more attention, compared to them, alumina as a host is of better thermal stability, durability and anti-chemical-corrosion [24]. The alumina would serve in worse environment, and at the same time, it was the main raw materials to prepare the garnet compositions such as YAG and $Yb_3Al_5O_{12}$ (YbAG) [25,26] which possess excellent optical property, so the alumina would be a nice host material for upconversion. In previous reports of upconversion materials, the rare earth ion Yb^{3+} is almost used as a doped ion rather than a composition of a compound. In this paper, we report pure red emission in Er^{3+} doped YbAG where Yb^{3+} is not only a composition of YbAG, but also a sensitizing ion.

2. Experimental details

Er^{3+} doped YbAGs were prepared with sol–gel method. 0.05 mol $Al(NO_3)_3{\cdot}9H_2O$ (analytic purity) was dissolved in 20 alcohol and the same molar citric acid was added as chelating agent and assistant solvent. Proportional Er_2O_3 and Yb_2O_3 (99.99%) powders were dissolved in 30 ml distilled water and then double molar citric acid of Ln^{3+} was added in. At room temperature, $Al(NO_3)_3$ solution was introduced slowly into the rare earth ions solution under vigorous stirring. At the end, the transparent solution was successfully prepared and kept for a week at room temperature, then the solution was dried at 100–120 °C. In the process of drying, no deposit was formed until all solvent was evaporated and the foamy gel was

* Corresponding author at: Institute of Modern Physics, Faculty of Material & Photoelectronic Physics, Xiangtan University, Xiangtan, Hunan 411105, China.
Tel.: +86 732 8292113.
E-mail address: yqb@xtu.edu.cn (Q. Yang).

0925-8388/$ – see front matter © 2010 Published by Elsevier B.V.
doi:10.1016/j.jallcom.2009.12.189

finally obtained. Then the gel was ground into fine homogeneous powder. The collected gel was heated at 500 °C for half an hour and kept at 1200 °C for 2 h. At last, the sintered substance was taken out of the furnace and cooled down to the room temperature in atmosphere. Three samples named with sample 1, sample 2 and sample 3 had been prepared with compositions of $Er^{3+}_x Yb^{3+}_{3-x}Al_5O_{12}$ (x = 0.45, 0.40 and 0.36).

X-ray diffraction (D/Max-Ra Cu kα, λ = 1.5406) and TEM (JEOL JEM2100 200 kV) were used to examine the phase structure and composition. The measurement of upconversion emission spectra of the as-prepared powder was performed at R-500 spectrometer at room temperature by excitation of 980 nm semiconductor laser diode with output power of 60 mW.

3. Results and discussion

3.1. Structure and composition analysis

Fig. 1 shows XRD patterns of the prepared powder at the sintering temperature of 1200 °C which reveal that two phases can be indexed to YbAG (JCPDS No. 73-1369) phase and Yb_2O_3 (JCPDS No. 48-1633) phase in all three samples. Because the diffraction peaks of $Er_3Al_5O_{12}$ (JCPDS No. 78-1451) and $Yb_3Al_5O_{12}$ overlap together and the ion radius of Er^{3+} (0.881 Å) is very close to that of Yb^{3+} (0.858 Å) so that Er^{3+} ion and Yb^{3+} ion can substitute for each other to form a common compound $(Er, Yb)_3Al_5O_{12}$. From the XRD patterns, the diffraction peaks of Yb_2O_3 are relatively strong, but that of Al_2O_3 were not found which probably existed as amorphous according to the stoichiometric concentration in the raw materials. Compared to the sample 2 and sample 3, the (2 2 2) diffraction peak of Yb_2O_3 in the sample 1 is higher than the (4 2 0) peak of YbAG which implied that more Yb_2O_3 grains formed in sample 1.

TEM pattern of the sample 2 shown in Fig. 2(a) indicates that the average size of the YbAG powder is about 300 nm. The particles of Yb_2O_3 disperse among YbAG grains marked with 1, 2, and 3. Fig. 2(b) and (c) shows the HRTEM images and selected area electron diffraction patterns (SAED) (insets of Fig. 2(b) and (c) of the two phases Yb_2O_3 and YbAG). Fig. 2(d) and (e) is EDS patterns of these two phases. The peak of Cu in EDS pattern is from the copper grid. Since the Er^{3+} ion radius is very close to that of Yb^{3+}, HRTEM patterns cannot distinguish Yb^{3+} from Er^{3+}. The results of EDS analysis shown in Fig. 2(d) and (e) and Table 1 prove that one of every four Yb^{3+} ions was replaced by one Er^{3+} ion at YbAG crystal. Phase Yb_2O_3 dissolved with Er_2O_3 has no upconversion emission due to the con-

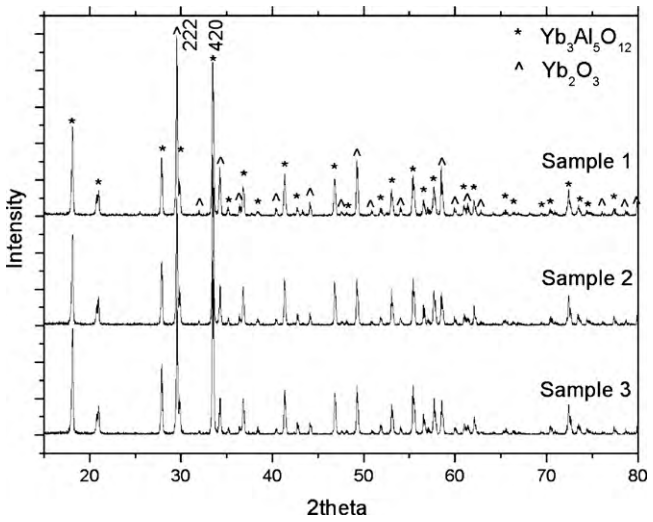

Fig. 1. The XRD pattern of the prepared powder sintered at 1200 °C.

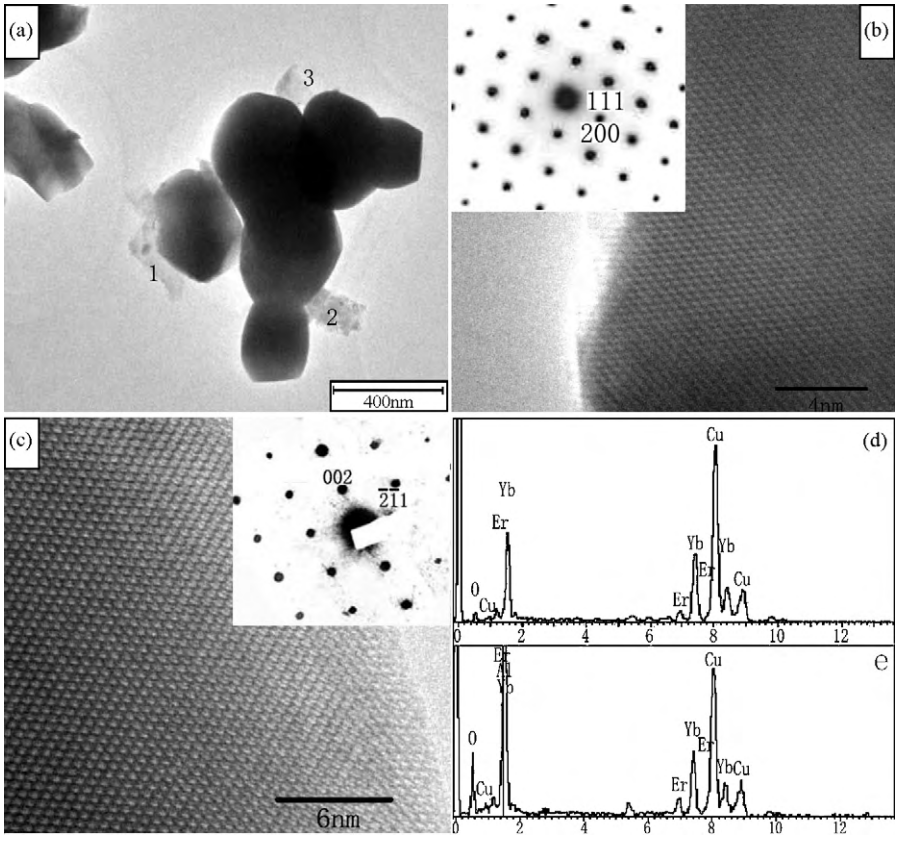

Fig. 2. TEM image of sample 2: (a) TEM micrograph of YbAG/Yb_2O_3, the crystal Yb_2O_3 disperses among YbAG grains marked with 1, 2, and 3; HRTEM images of Yb_2O_3 phase (b) and $Al_5Yb_3O_{12}$ phase (c) (the insets are the corresponding electron diffraction patterns); (d and e) EDS spectra of Yb_2O_3 phase and YbAG phase.

Table 1
Ingredients of two phases in sample 1.

Yb_2O_3 phase		YbAG phase	
Element	at.%	Element	at.%
O K	21.35	O K	40.59
Er L	10.15	Al K	34.41
Yb L	68.50	Er L	5.19
Total	100.00	Yb L	19.81
		Total	100.00

centration quench [9]. It can be concluded that the upconversion emission must be generated from YbAG phase.

3.2. Upconversion emission

The red emission was observed by naked eyes when the prepared powder was excited with 980 nm LD even the exciting power as low as 10 mW. Fig. 3 shows the upconversion spectra of the prepared powders in the wavelength range of 500–850 nm. The difference of emission spectra of these three samples is not obvious. The red upconversion emission band is centered at 625–725 nm and the green one at 525–567 nm. The red band consists of at least 10 sharp peaks due to Stark split lying at 652, 655, 662, 665, 670, 678 and 685 nm. The integrated intensity ratios of the red emission (integration area is 625–725 nm) to the green one (integration area is 500–600 nm) in three samples are 78, 136 and 110, respectively, which account for the high purity of red emission. The ratio R/G is positively variation with the concentration ratio of Yb^{3+}/Er^{3+} that can be seen from Fig. 3.

There were many papers to explain the upconversion emission mechanism for Er^{3+} doped or Er^{3+}/Yb^{3+} co-doped materials. Most of the explanations are almost the same, so that we explain upconversion mechanism first briefly, then discuss mechanism of the pure red emission.

The possible upconversion mechanisms are illustrated by the simplified energy level of Er^{3+} and Yb^{3+} shown in Fig. 4. The population of $^4I_{11/2}$ of Er^{3+} is excited with 980 nm LD mainly by energy transfer (ET) of Yb^{3+} and partially by the ground state absorption (GSA) of Er^{3+} itself: $^2F_{5/2}(Yb^{3+}) + {}^4I_{15/2}(Er^{3+}) \rightarrow {}^2F_{7/2}(Yb^{3+}) + {}^4I_{11/2}(Er^{3+})$ and $^4I_{15/2}(Er^{3+}) + a\ 980\ photon \rightarrow {}^4I_{11/2}(Er^{3+})$. The next step involves the excitation processes based on the long-lived $^4I_{11/2}$ level as follows:

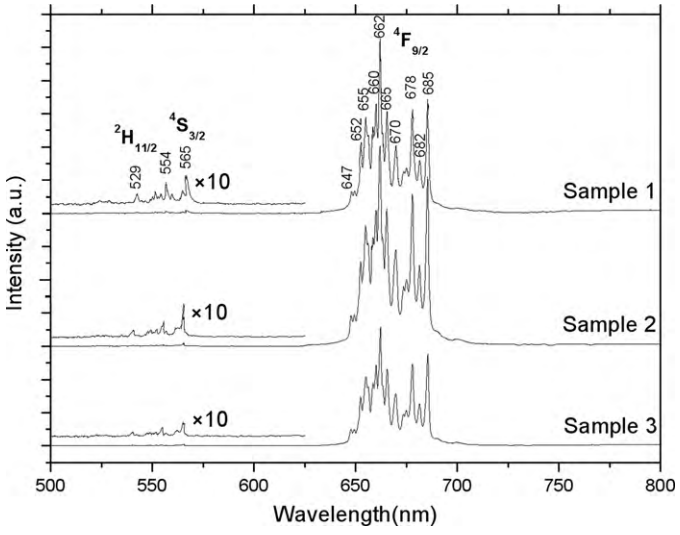

Fig. 3. The upconversion emission spectra of three samples excited with 980 nm laser diode.

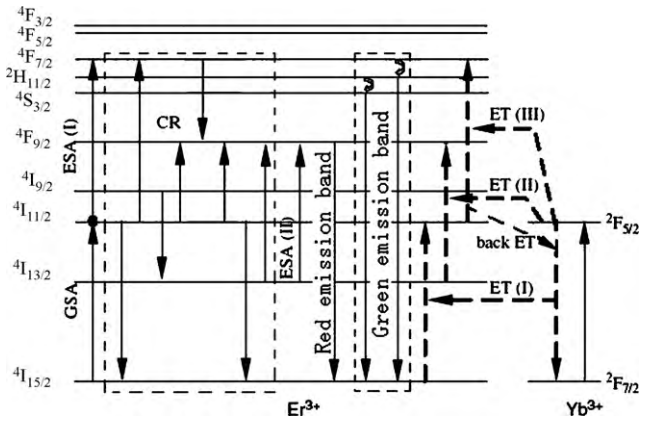

Fig. 4. The simplified energy level diagram of Yb^{3+} and Er^{3+}.

(1) Cross relaxation (CR) $^4I_{11/2}(Er^{3+}) + {}^4I_{11/2}(Er^{3+}) \rightarrow {}^4I_{15/2}(Er^{3+}) + {}^4F_{7/2}(Er^{3+})$.
(2) The excited state absorption (ESA) of Er^{3+}: $^4I_{11/2} + a\ photon \rightarrow {}^4F_{7/2}$.

The populated $^4F_{7/2}$ (Er^{3+}) level then relaxes nonradiatively and rapidly to the next lower levels $^2H_{11/2}$ and $^4S_{3/2}$. The above processes will produce the $^2H_{11/2} \rightarrow {}^4I_{15/2}$ and $^4S_{3/2} \rightarrow {}^4I_{15/2}$ green emissions centered at 525 and 546 nm respectively.

The red emission centered around 657 nm is originated from the transition $^4F_{9/2} \rightarrow {}^4I_{15/2}$.

$^4F_{9/2}$ is populated based on following processes:

(1) $^4I_{11/2}$ (Er^{3+}) nonradiative relaxation to $^4I_{13/2}(Er^{3+})$.
(2) ET (II) from Yb^{3+}: $^2F_{5/2}$ $(Yb^{3+}) + {}^4I_{13/2}$ $(Er^{3+}) \rightarrow {}^4F_{9/2}$ $(Er^{3+}) + {}^2F_{7/2}(Yb^{3+})$.
(3) CR between Er^{3+} ions: $^4I_{13/2} + {}^4I_{11/2} \rightarrow {}^4I_{15/2} + {}^4F_{9/2}$.
(4) ESA $^4I_{13/2} + a\ photon \rightarrow {}^4F_{9/2}$.

It is well known that the Er^{3+} doped materials usually emit green and red lights and the green is stronger than the red in most cases. From practical point of view, sometimes pure and strong red emissions are needed. Yb^{3+} usually is doped as a sensitizing ion to enhance the efficiency of the upconversion emission of Er^{3+}, however, in addition to the enhancement of the efficiency, Yb^{3+} has the ability to realize pure red emission. It is well known that red emission is due to energy level transition from $^4F_{9/2}$ to $^4I_{15/2}$ and green one due to $^2H_{11/2}$ and $^4S_{3/2}$ to $^4I_{15/2}$. To explain the mechanism for Yb^{3+} increasing the ratio of red to green, we start from Dexter's formulation [24].

$$P(R)\alpha\frac{Q_A}{R^b\tau_D}\int\frac{f_D(E)F_A(e)}{E_c}dE \quad (1)$$

where τ_D is the decay time of the donor emission which usually decreases in the case of Yb^{3+}/Er^{3+} co-doped, Q_A the total absorption cross-section of the acceptor ion, R the distance between the donor and the accepter and b and c are the parameters dependent on the type of energy transfer. The probability functions $f_D(E)$ and $F_A(e)$ represent the observed shapes of the donor emission band and the acceptor absorption band respectively. According to Eq. (1), it is very clear that the energy transfer rate $P(R)$ is in inverse variation to the distance R between the donor and the acceptor and the decay time. The increase of Yb^{3+} content in the neighbor environment of Er^{3+} shortened the distance R between Yb^{3+} and Er^{3+} ions and decreased the decay time that would promote these transitions $^4I_{15/2}(Er^{3+}) \rightarrow {}^4I_{11/2}(Er^{3+})$, $^4I_{11/2}(Er^{3+}) \rightarrow {}^4F_{7/2}(Er^{3+})$ and $^4F_{7/2}(Er^{3+}) + {}^4I_{11/2}(Er^{3+}) \rightarrow 2{}^2F_{9/2}(Er^{3+})$, where $^4F_{7/2}(Er^{3+}) +$

$^4I_{11/2}(Er^{3+}) \rightarrow 2^2F_{9/2}(Er^{3+})$ is a resonant energy transfer according to energy level calculation [8]. When the sample doped with only Er^{3+}, the population of $^4I_{11/2}(Er^{3+})$ is mainly built via GSA of Er^{3+}. Due to the relatively lower cross-section absorption, the population of $^4I_{11/2}$ (Er^{3+}) is much less than that of the population of $^4F_{7/2}(Er^{3+})$. The process $^4F_{7/2}(Er^{3+}) + {}^4I_{11/2}(Er^{3+}) \rightarrow 2^2F_{9/2}(Er^{3+})$ means that one electron in the $^4F_{7/2}(Er^{3+})$ needs a matching electron in the $^4I_{11/2}(Er^{3+})$, thus the process $^4F_{7/2}(Er^{3+}) + {}^4I_{11/2}(Er^{3+}) \rightarrow 2^2F_{9/2}(Er^{3+})$ is very weak. When the content of Yb^{3+} increased, the population of $^4I_{11/2}(Er^{3+})$ will increase remarkably by the ET of Yb^{3+} $^2F_{5/2}(Yb^{3+}) + {}^4I_{15/2}(Er^{3+}) \rightarrow {}^2F_{7/2}(Yb^{3+}) + {}^4I_{11/2}(Er^{3+})$ and finally the process $^4F_{7/2}(Er^{3+}) + {}^4I_{11/2}(Er^{3+}) \rightarrow 2^2F_{9/2}(Er^{3+})$ becomes very strong and therefore red emission is greatly enhanced. It should be pointed out that the Yb^{3+} in our experiment is not a dopant ion but a composition of the host, however it still plays the sensitizing role verified by the luminescence spectra. Another reason for green emission quenching is the intensive cross relaxation between Ytterbium ion and Erbium ion due to high Yb^{3+} concentration.

4. Conclusions

The powders of YbAG/Yb_2O_3 were prepared by sol–gel method. XRD and TEM analysis revealed that the as-prepared samples consisted of two co-existed phases of YbAG and Yb_2O_3. Pure red emissions in three samples with R/G = 78, 110 and 136 were obtained and the R/G values are in positively variation to the ratio of Yb^{3+}/Er^{3+}. The possible emission mechanism can be ascribed to the resonant energy transfer $^4F_{7/2}(Er^{3+}) + {}^4I_{11/2}(Er^{3+}) \rightarrow 2^2F_{9/2}(Er^{3+})$ caused by the high content of Yb^{3+}. This pure red emission of as-prepared material will have potential application in color display.

Acknowledgement

This work was supported by Hunan Education Department Foundation of China (Grant No. 06C818).

References

[1] T.J. Whitley, C.A. Millar, R. Wyatt, M.C. Brierley, D. Szebesta, Electron. Lett. 27 (1991) 1785.
[2] G. Lakshminarayana, J. Qiu, J. Alloy Compd. 476 (2009) 720.
[3] E. Downing, L. Hesselink, J. Ralston, R. Macfarlane, Science 273 (1996) 1185.
[4] S. Xu, Z. Yang, S. Dai, G. Wang, L. Hu, Z.H. Jiang, Mater. Lett. 58 (2004) 1026.
[5] H. Hayashi, S. Tanabe, N. Sugimoto, J. Lumin. 128 (2008) 333.
[6] R. Gao, Y. Zhang, P. Gopalakrishnakone, Biotechnol. Progr. 24 (2008) 245.
[7] M. D' Zmura, Vision Res. 31 (1991) 951.
[8] B. Dong, C. Li, M. Lei, J. Lumin. 126 (2007) 441.
[9] Y.X. Liu, Q.B. Yang, G.Z. Ren, C.F. Xu, Y. Zhang, J. Alloy Compd. 467 (2009) 351.
[10] F. Vetrone, J.C. Boyer, J.A. Capobianco, A. Speghini, M. Bettinilli, J. Appl. Phys. 96 (2004) 661.
[11] S. Xiao, X. Yang, Z. Liu, X. Yan, Opt. Mater. 28 (2006) 285.
[12] D. Matsuura, Appl. Phys. Lett. 81 (2002) 4526.
[13] M. Liu, S.W. Wang, J. Zhang, L.Q. An, L.D. Chen, Opt. Mater. 29 (2007) 1352.
[14] Y.F. Bai, Y.X. Wang, G.Y. Peng, K. Yang, X.R. Zhang, Y.L. Song, J. Alloy Compd. 478 (2009) 676.
[15] Y.Q. Sheng, L.L. Xu, J. Liu, D. Zhai, Z.G. Zhang, J. Alloy Compd. 130 (2010) 338.
[16] Y.H. Li, G.Y. Hong, Y.M. Zhang, Y.N. Yu, J. Alloy Compd. 456 (2008) 247.
[17] J. Zhang, L.Q. An, S.W. Wang, J. Alloy Compd. 471 (2009) 201.
[18] Y.H. Wang, J. Ohwaki, Appl. Phys. Lett. 63 (1993) 3268.
[19] X. Shen, Q.H. Nie, T.F. Xu, T. Peng, Y. Gao, Phys. Lett. A 332 (2004) 101.
[20] J. Silver, M.I. Martinez-Rubio, T.G. Fern, R. Withnall, J. Phys. Chem. B 105 (2001) 948.
[21] J.F. Suyver, J. Grimm, M.K. Van Veen, D. Biner, et al., J. Lumin. 117 (2006) 1.
[22] D.K. Ma, S.M. Huang, Y.Y. Yu, Y.F. Xu, Y.Q. Dong, J. Phys. Chem. C 113 (2009) 8136.
[23] H.X. Yang, H. Lin, L. Lin, Y.Y. Zhang, B. Zhai, E.Y.B. Pun, J. Alloy Compd. 453 (2008) 493.
[24] T. Danger, J. Koetke, R. Brede, E. Heumann, G. Huber, B.H.T. Chai, J. Appl. Phys. 76 (1994) 1413.
[25] M. Kaczkan, M. Borowska, K. Kołodziejak, T. Łukasiewicz, M. Malinowski, Opt. Mater. 30 (2008) 703.
[26] D.J. Dexter, J. Chem. Phys. 21 (1953) 836.